Civil Engineering Sciences
A SCIENCE PARTNER JOURNAL

RESEARCH ARTICLE

A Magnitude-Based Incremental Dynamic Analysis Method for Seismic Performance Assessment of Near-Fault Structures

Chao Luo[1,2], Jingjing Li[1], Hao Wang[1,2*], Xueliang Rong[1,2], and Xiaoshan Wang[3]

[1]School of Civil Engineering, Shijiazhuang Tiedao University, Shijiazhuang 050043, China. [2]Key Laboratory of Roads and Railway Engineering Safety Control, Ministry of Education, Shijiazhuang Tiedao University, Shijiazhuang 050043, China. [3]Hebei Earthquake Agency, Shijiazhuang 050021, China.

*Address correspondence to: wanghao@stdu.edu.cn

Citation: Luo C, Li J, Wang H, Rong X, Wang X. A Magnitude-Based Incremental Dynamic Analysis Method for Seismic Performance Assessment of Near-Fault Structures. *Civil Eng. Sci.* 2026;2:Article 0011. https://doi.org/10.34133/cesci.0011

Submitted 15 September 2025
Revised 26 November 2025
Accepted 30 November 2025
Published 29 January 2026

Seismic performance assessment of near-fault critical structures remains challenging, as conventional intensity-based incremental dynamic analysis (IDA) approaches suffer from subjective ground motion selection and nonphysical amplitude scaling, which introduce artificial dispersion and compromise performance assessment reliability. This study proposes a magnitude-based incremental dynamic analysis (MIDA) method that replaces empirical record selection and scaling with physically consistent ground motion simulations conditioned on earthquake magnitude. Various earthquake scenarios, ranging from service level to maximum considered earthquakes, are simulated, and the curvature ductility ratio at the tower base is adopted as the damage measure to evaluate the seismic performance of a near-fault cable-stayed bridge. Results indicate that MIDA yields markedly lower dispersion and improved physical consistency in structural responses than IDA after entering the nonlinear stage. In maximum credible earthquake scenarios, the coefficient of variation of structural response reaches 95.3% in IDA but is only 51.5% in MIDA, highlighting the improved reliability and accuracy of seismic performance assessment. By addressing the critical limitations of conventional IDA approaches, MIDA substantially enhances the physical consistency and precision of seismic performance assessments for near-fault structures. It offers a scalable methodological basis for consistent seismic performance evaluation and supports reliability-informed engineering decision-making in near-fault hazard zones.

Introduction

Evaluating seismic performance is essential for structural design, risk mitigation, and resilience, especially in areas prone to strong ground motions. This is crucial for structures near active faults, where seismic input characteristics can vary markedly. Over the past decades, incremental dynamic analysis (IDA) has been widely adopted for its intuitive representation of structural response to increasing seismic intensity and utility in fragility analysis [1–5]. However, IDA exhibits inherent limitations that constrain its ability to accurately represent real-world seismic scenarios despite its popularity. Specifically, IDA relies heavily on the selection and amplitude scaling of historical ground motion records [6–10], introducing subjectivity and possibly distorting the frequency content and energy characteristics of input motions. This potentially results in structural response overestimation or underestimation [11]. Ground motion records used in IDA are typically obtained from past earthquakes that reflect site- and source-specific conditions not necessarily aligned with those of a target site, especially in near-fault regions. Consequently, the extent to which IDA outputs can reliably represent the true seismic performance of structures is of increasing concern. Therefore, the validity and reasonableness of the assumption that scaled records can represent actual seismic scenarios in IDA remain questionable. Besides these limitations, current IDA frameworks rarely account for magnitude variations in specific scenarios or employ ground motion inputs consistent with seismic hazard characteristics. This leaves a critical gap in accurately evaluating the seismic performance of engineering structures in realistic earthquake scenarios.

Near-fault ground motions are often characterized by short durations, pronounced velocity pulses, and fling-step effects. These features tend to amplify structural seismic demands, posing considerable challenges for critical structures located near-fault lines. Existing studies have shown that near-fault ground motion records can increase seismic demands by approximately 10% of those of far-field ground motions [12,13]. In IDA, the effects of near-fault ground motions are typically considered by selecting ground motion records that exhibit pulse-like or fling-step characteristics [14,15]. However, such characteristics are more commonly observed in moderate-to-large-magnitude earthquakes [16,17], and not all near-fault ground motions exhibit pulse-like characteristics [16]. Therefore, the validity of conducting IDA using only scaled pulse-like near-fault records

has been questioned [18,19]. There is a growing need for techniques that can directly incorporate earthquake source parameters and site effects in generating ground motion inputs for seismic performance evaluation.

Considering the above issues, some studies have employed physics-based ground motion simulations, comprehensively incorporating source mechanisms and regional geological conditions, and they hold important application promise in earthquake engineering [20–26]. Previous studies have proposed a fault-to-structure simulation approach that uses physics-based ground motion simulations incorporating site- and source-specific conditions [27,28]. This approach allows for realistic ground motion propagation from the seismic source to the structure, facilitating accurate structural response analysis. Related studies have also employed physics-based simulations to generate ground motions for seismic fragility analysis, demonstrating the applicability of such methods for assessing regional seismic vulnerability and risk [29]. Although physics-based ground motion simulation methods address the subjectivity in selecting ground motion records and the amplitude scaling effects, most research has predominantly focused on structural response analysis. There is an urgent need to integrate these methods into the assessment of structural seismic performance.

To address the aforementioned gaps, this study proposes a magnitude-based incremental dynamic analysis (MIDA) method that employs physics-based ground motion simulations to generate inputs representative of actual site conditions and seismic source characteristics. Unlike the IDA approach, which depends on scaling historical ground motion records, the MIDA method takes a source-to-site-to-structure perspective by using earthquake magnitude to represent seismic scenarios with different exceedance probabilities and simulates ground motions corresponding to various magnitudes. Considering a near-fault cable-stayed bridge as a case study, this study investigates the advantages of the MIDA method over IDA by comparing their results. This study provides critical insights that advance the current understanding of seismic performance assessment for engineering structures.

Materials and Methods

MIDA procedure

The MIDA method performs incremental near-fault ground motion simulations for a bridge structure based on increasing earthquake magnitudes. In particular, it evaluates structural seismic performance by incrementally simulating near-fault ground motions corresponding to increasing earthquake magnitudes. In this study, a sequence of 11 magnitude levels was considered, including 4.8 (service level earthquake), 4.9, 5.1, 5.3, 5.5 (design basis earthquake), 5.7, 5.9 (maximum considered earthquake), 6.1, 6.3, 6.5, and 6.8 (maximum credible earthquake). Within each simulated ground motion field, input records were selected based on the spatial relationship between the structure site and fault rupture. When the structure lies directly above the rupture trace area, i.e., Joyner–Boore distance ($R_{JB} = 0$), all ground motions within the surface projection of the fault rupture were included. When $R_{JB} > 0$, ground motions were selected from the side of the structure site where $R_{JB} > 0$, ensuring that the selected records fall within the fault length in the strike-parallel direction or the width in the strike-perpendicular direction. The simulated ground motions were applied to time history analyses, and the bridge dynamic responses were computed for each magnitude-specific ground motion dataset.

An appropriate structural damage measure (DM) was selected to evaluate the seismic performance of the structure. In this study, DM is defined as the curvature ductility ratio at the tower base around the bridge longitudinal rotational axis [30,31]. The median DM value of each earthquake magnitude M, denoted as M_{DM}, was extracted. A MIDA curve under near-fault ground motions can be constructed by plotting the set of coordinate pairs (M, M_{DM}) and connecting them. It is assumed that the DM–M relationship follows a lognormal distribution. For each magnitude M, the median DM value and the standard deviation of the logarithmic DM values, δ_{DM}, were obtained. Based on these parameters, the 50th, 84th, and 16th percentile curves [32] were constructed as (M, M_{DM}), [M, M_{DM}·exp(δ_{DM})], and [M, M_{DM}·exp ($-\delta_{DM}$)], respectively. Figure 1 shows the overall MIDA procedure.

Project overview and computational model

This study focuses on a single-pylon cable-stayed bridge with a fully floating structural system. The main bridge has a total length of 380 m and a pylon height of 146.5 m. Figure 2A shows the bridge's general layout. The main girder is a steel box girder fabricated from Q345 steel. The pylon comprises 3 distinct segments: a steel segment, a concrete segment, and a hybrid steel–concrete segment located between the steel and concrete segments, as shown in Fig. 2B. The steel segment is made of Q420 steel, the concrete segment uses C40 concrete, and the hybrid steel–concrete segment employs C50 concrete. The concrete and hybrid steel–concrete segments have elliptical cross-sections, as depicted in Fig. 2C and D.

A 3-dimensional finite element model of the cable-stayed bridge was established using Midas Civil to accurately represent the structural configuration and mechanical behavior based on the engineering design data. According to Kuhlemeyer and Lysmer [33], the element mesh should not exceed 1/8 of the minimum wavelength of the simulated seismic motion for wave propagation simulations using finite element methods. In this study, the minimum shear wave velocity of the site is 2,260 m/s, the maximum simulated seismic motion frequency is 5 Hz, and the minimum simulated seismic motion wavelength is 56.5 m. The calculation model's mesh size is set to 1.8 m to minimize mesh size effects. The first natural period of the bridge is $T_1 = 2.52$ s. The main girder and steel segment of the pylon were simulated using elastic beam elements, whereas the concrete and hybrid segments were modeled using fiber-based nonlinear beam elements to capture inelastic behavior. Cross-section discretization included cover concrete, confined concrete, and longitudinal reinforcement. The reinforcement steel was modeled using a bilinear stress–strain constitutive relationship, while both unconfined and confined concrete were modeled using the Mander constitutive model. The transverse and vertical displacements of the main girder were coupled with those of the auxiliary and side piers at one end, whereas only the vertical displacement was coupled at the other end. The pylon base was modeled as a fixed support.

Physics-based simulation of near-fault ground motions

In this study, ground motion simulations were performed using the finite-difference software SW4 (Seismic Waves, Fourth Order) [34–36], which allows for high-resolution wavefield modeling in complex geological media. The fault rupture was

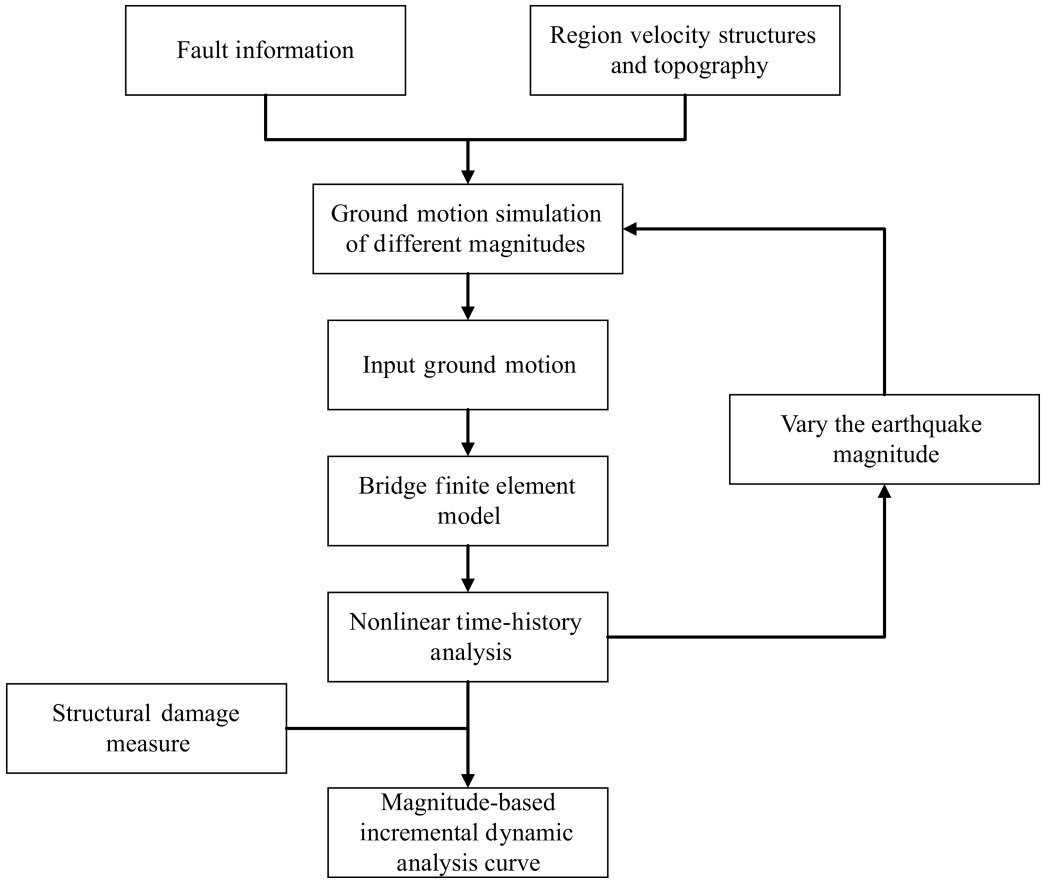

Fig. 1. Fundamental process of MIDA.

modeled using the GP (Graves and Pitarka) kinematic rupture model [37–42], which provides physically realistic source–time functions and spatially variable slip distributions. The fault is characterized by a dip angle of 50°, a rake angle of −90°, and a strike oriented in the northwest direction, corresponding to a normal faulting mechanism. Table 1 presents the one-dimensional (1D) velocity model information.

Given that the cable-stayed bridge has an R_{JB} of 2 km and is located on the footwall side, a ground motion collection region was defined to account for near-fault effects based on the fault rupture's spatial configuration. The relative spatial positions of the fault and ground motion collection area are shown in Fig. 3. The bridge is assumed to experience ground motions within $0 < R_{JB} \leq 2$ km and within the limits defined by the 31 km fault length in the strike-parallel direction. Consequently, the region encompassing the 31 km fault length in the strike-parallel direction and extending 2 km from the fault trace toward the footwall side in the strike-normal direction is designated as the ground motion collection area for the bridge site.

Determination of fault rupture parameters

Peak ground acceleration (PGA) values corresponding to different seismic hazard levels were determined according to the site classification specified in the China seismic ground motion parameter zonation map (GB18306-2015) [43]. The PGA values obtained for service level, design basis, and maximum considered earthquakes were 0.03*g*, 0.1*g*, and 0.19*g*, respectively. These values were converted to seismic intensities using an empirical PGA–intensity correlation proposed by Zhang [44], which correlates PGA with seismic intensity as follows:

$$I = 3.23 \lg \mathrm{PGA} + 6.82 \tag{1}$$

where I denotes the seismic intensity corresponding to the PGA. Then, the earthquake magnitudes can be calculated from seismic intensities using the empirical relationship between epicentral intensity and magnitude proposed by Li [45]. The empirical equation is expressed as follows:

$$M_S = 0.58I + 1.5 \tag{2}$$

where M_S denotes the corresponding surface wave magnitude. The surface wave magnitude (M_S) was then converted to moment magnitude (M_W) using the empirical relationship between M_S and M_W based on the statistical analysis of data from the China Seismic Network [46]. The conversion equation is given as follows:

$$M_W = 0.805M_S + 1.154 \tag{3}$$

The surface rupture length (SRL) and rupture width (RW) were calculated using the empirical relationships for normal faulting events [47]. The equations are expressed as follows:

$$\lg \mathrm{SRL} = -2.01 + 0.5M_W \tag{4}$$

$$\lg \mathrm{RW} = -1.14 + 0.35M_W \tag{5}$$

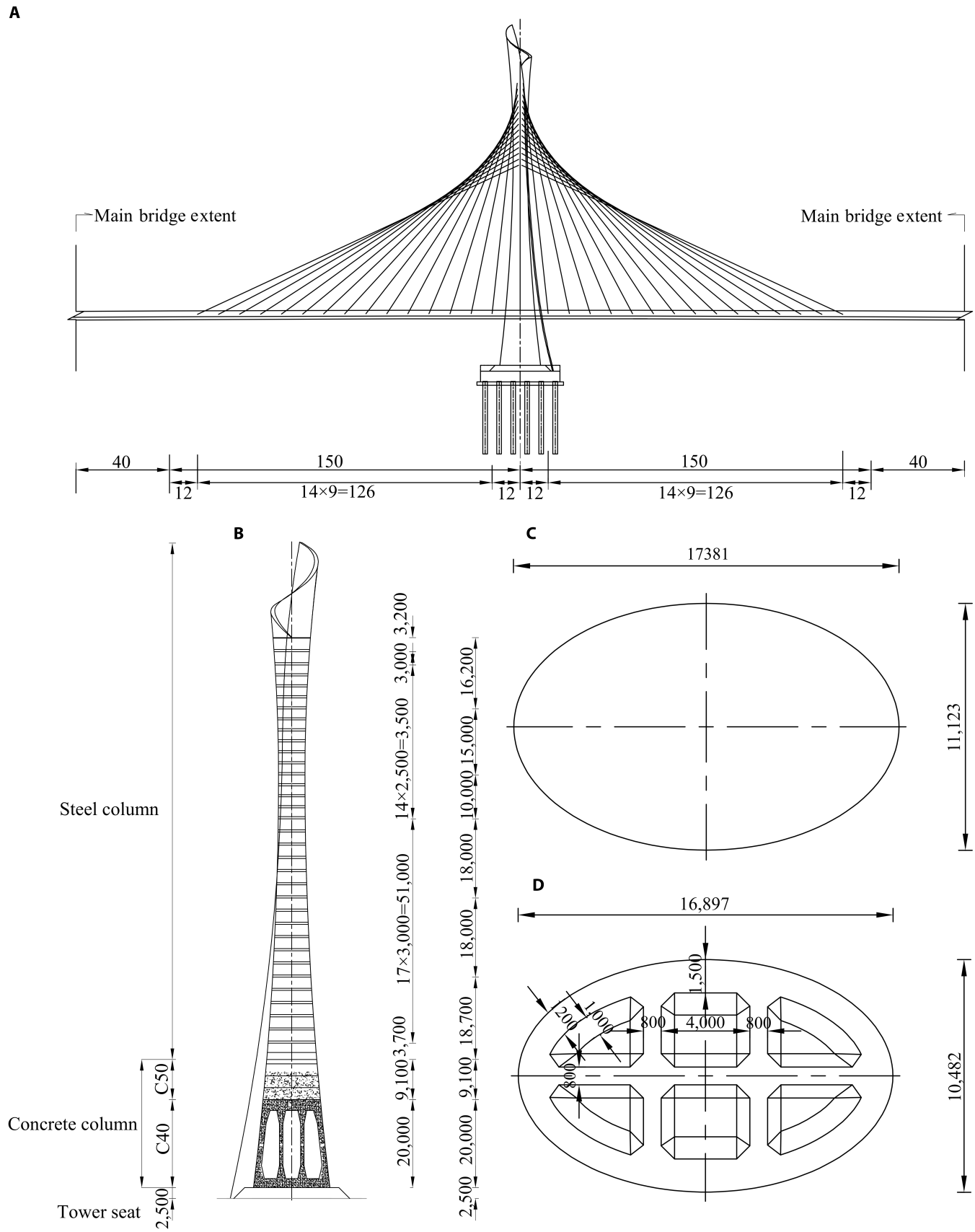

Fig. 2. General bridge layout and bridge tower configuration: (A) general bridge layout (m), (B) bridge tower elevation (mm), (C) cross-section of concrete tower column (mm), and (D) cross-section of the hybrid steel–concrete tower column (mm).

Table 1. 1D velocity model information

Soil layer depth (km)	Shear wave velocity (km/s)	Compressional wave velocity (km/s)	Density (kg/m^3)	Quality factor Q_s	Quality factor Q_p
0.00	2.86	4.79	2,110	286	143
5.00	3.35	5.72	2,760	335	168
10.00	3.52	5.95	2,760	352	176
15.00	3.60	6.07	2,810	360	180
20.00	3.65	6.26	2,810	365	183
30.00	3.93	6.68	2,910	393	197

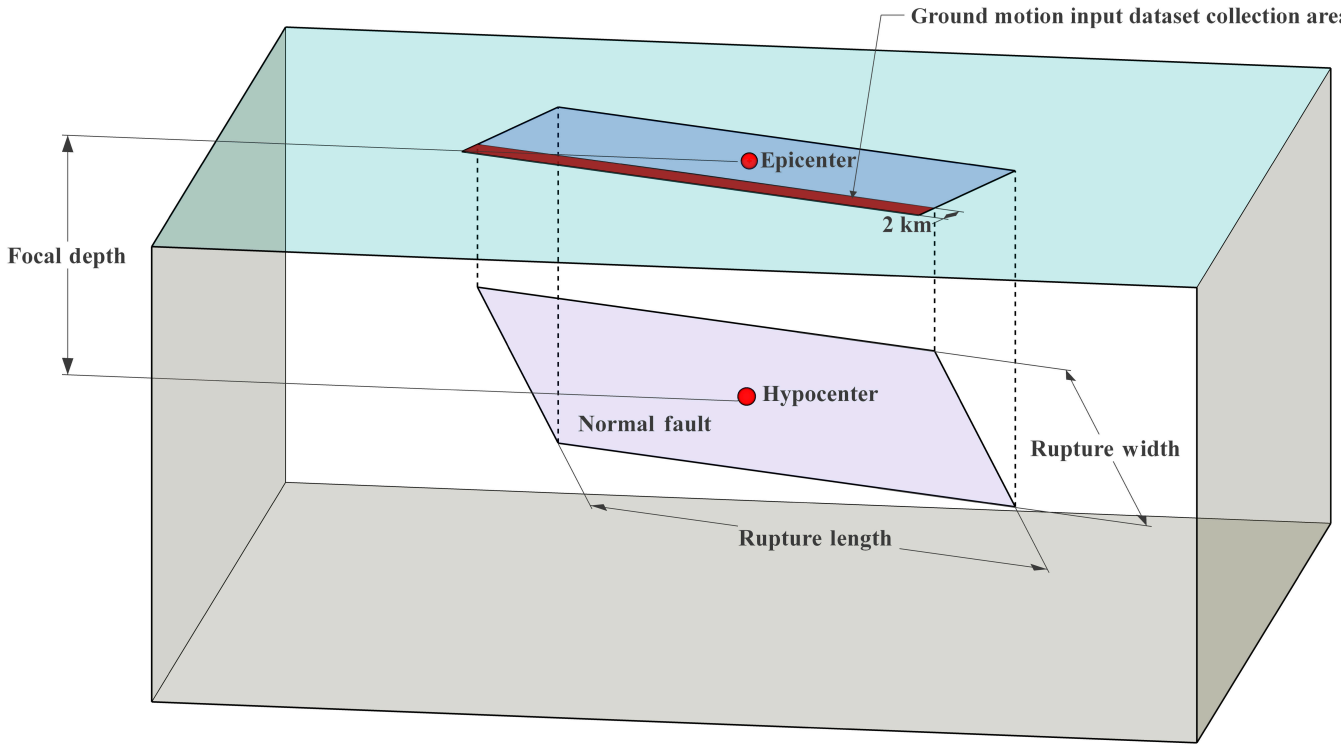

Fig. 3. Relative location diagram of fault and ground motion collection area. The red rectangle indicates the ground motion input dataset collection area.

To estimate the earthquake magnitude and RW associated with the maximum credible earthquake, the seismic source was assumed to have reached its maximum capacity, and the full fault length was considered as the SRL. Based on the empirical relationships for normal faulting events [47], the moment magnitude of the maximum credible earthquake was first calculated from the SRL as follows:

$$M_W = 4.86 + 1.32 \lg \mathrm{SRL} \quad (6)$$

Subsequently, the surface RW was calculated using Eq. 5.

Ground motion selection and scaling in IDA

In this study, the acceleration response spectrum of the engineering site was determined according to the code for seismic design of highway bridges [48]. The site was classified as Type II, with the shear wave velocity of the soil layers ranging from 500 to 2,000 m/s. Ground motion records meeting these criteria were selected from the strong motion database of the Pacific Earthquake Engineering Research Center [49]. Among the ground motions satisfying the above criteria, 22 recorded ground motions whose response spectra exhibited minimal deviation from the code-specified target spectrum at the bridge's fundamental periods in the longitudinal and transverse directions were selected. Figure 4 shows the normalized acceleration response spectra of the selected records.

For each of the 22 records, the horizontal component with the largest PGA was designated as the principal input direction. All 3 components of each ground motion were uniformly scaled based on this PGA. The scaled PGA levels included 0.033g (service level earthquake; $g = 9.81$ m/s^2), 0.100g (design basis earthquake), 0.190g (maximum considered earthquake), and 0.723g (maximum credible earthquake), as well as a set of intermediate values ranging from 0.200g to 2.000g in increments of 0.100g.

To construct the conventional IDA curve, nonlinear time history analyses were conducted at each PGA level.

Results

Seismic performance evaluation using MIDA

IDA is a parametric method for seismic performance assessment, in which ground motion records are scaled according to a selected intensity measure (IM), such as PGA and spectral acceleration Sa (T1, ξ). This study proposes the MIDA method to overcome the subjectivity in record selection and the limitations associated with amplitude scaling. In MIDA, earthquake magnitude replaces conventional IMs to represent seismic scenarios with different exceedance probabilities. A series of near-fault ground motion fields with increasing magnitudes is simulated, and the structural response is computed in each magnitude scenario. This allows for a comprehensive evaluation of the evolution of structural performance as seismic demand increases. The proposed MIDA method differs fundamentally from the traditional IDA approach in 2 key aspects: (a) it uses earthquake magnitude to represent seismic scenarios with varying exceedance probabilities instead of relying on conventional IMs, and (b) it employs physics-based, region-specific simulated ground motions instead of scaled historical records. These features allow MIDA to deliver a realistic, scenario-consistent method for evaluating the seismic performance of critical structures.

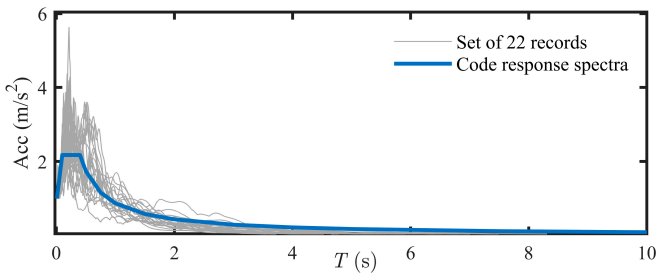

Fig. 4. Normalized acceleration response spectra of 22 recorded ground motions.

Ground motion field distribution characteristics

The Hutuo River Fault, located near the bridge site, has a total length of 31 km. Ground motion fields were simulated for 11 magnitudes, ranging from service level events to the maximum credible earthquake, to capture the influence of various potential seismic scenarios on a cable-stayed bridge. These scenarios are consistent with the China seismic ground motion parameter zonation map (GB18306-2015) [43], covering the service level earthquake (i.e., 63% exceedance probability in 50 years), the design basis earthquake (i.e., 10% exceedance probability in 50 years), the maximum considered earthquake (i.e., 2% exceedance probability in 50 years), and the maximum credible earthquake. For each scenario, the median, mean, standard deviation, and coefficient of variation (COV) of PGA values are summarized in Table 2, and the ShakeMaps (the spatial distribution of 3-component synthesized PGA) are shown in Fig. 5.

Notably, the average PGA values obtained from simulations progressively approach the PGA specified in the China seismic ground motion parameter zonation map (GB18306-2015) [43] with increasing earthquake magnitude. Under the maximum considered earthquake scenario with a magnitude of 5.95, the average PGA is approximately the code value, with a deviation of only 0.526%. This validates the effectiveness of the physics-based simulation approach in accurately representing site-specific ground motion intensities required for seismic performance assessments.

Comparison of MIDA and IDA results

In this study, MIDA and IDA use the curvature ductility ratio around the longitudinal rotational axis at the tower base as the DM [30,31]. Based on the structural performance classification criteria proposed by Hose et al. [50], this study used a 4-level damage classification: slight, moderate, extensive, and complete damage levels. Table 3 summarizes the quantitative information on the curvature ductility ratio for the damage states at the main tower base. Analyses are conducted for the bridge structure using MIDA and IDA, and the corresponding scatter plots of the curvature ductility ratio at the tower base obtained from both methods are shown in Fig. 6.

Table 2. Acceleration statistic information at different magnitudes

Magnitude, M_w	Code value (g [a])	Median (g)	Mean (g)	Standard deviation	Coefficient of variation
4.8 (service level earthquake)	0.033	0.032	0.069	0.089	1.299
4.9	–	0.040	0.075	0.086	1.156
5.1	–	0.045	0.097	0.117	1.211
5.3	–	0.071	0.116	0.123	1.058
5.5 (design basis earthquake)	0.100	0.076	0.125	0.131	1.044
5.7	–	0.106	0.135	0.122	0.898
5.9 (maximum considered earthquake)	0.190	0.179	0.191	0.096	0.503
6.1	–	0.203	0.216	0.109	0.505
6.3	–	0.236	0.259	0.124	0.477
6.5	–	0.388	0.396	0.120	0.304
6.8 (maximum credible earthquake)	–	1.076	1.059	0.187	0.177

[a]g refers to the gravitational acceleration, equivalent to 9.81 m/s^2.

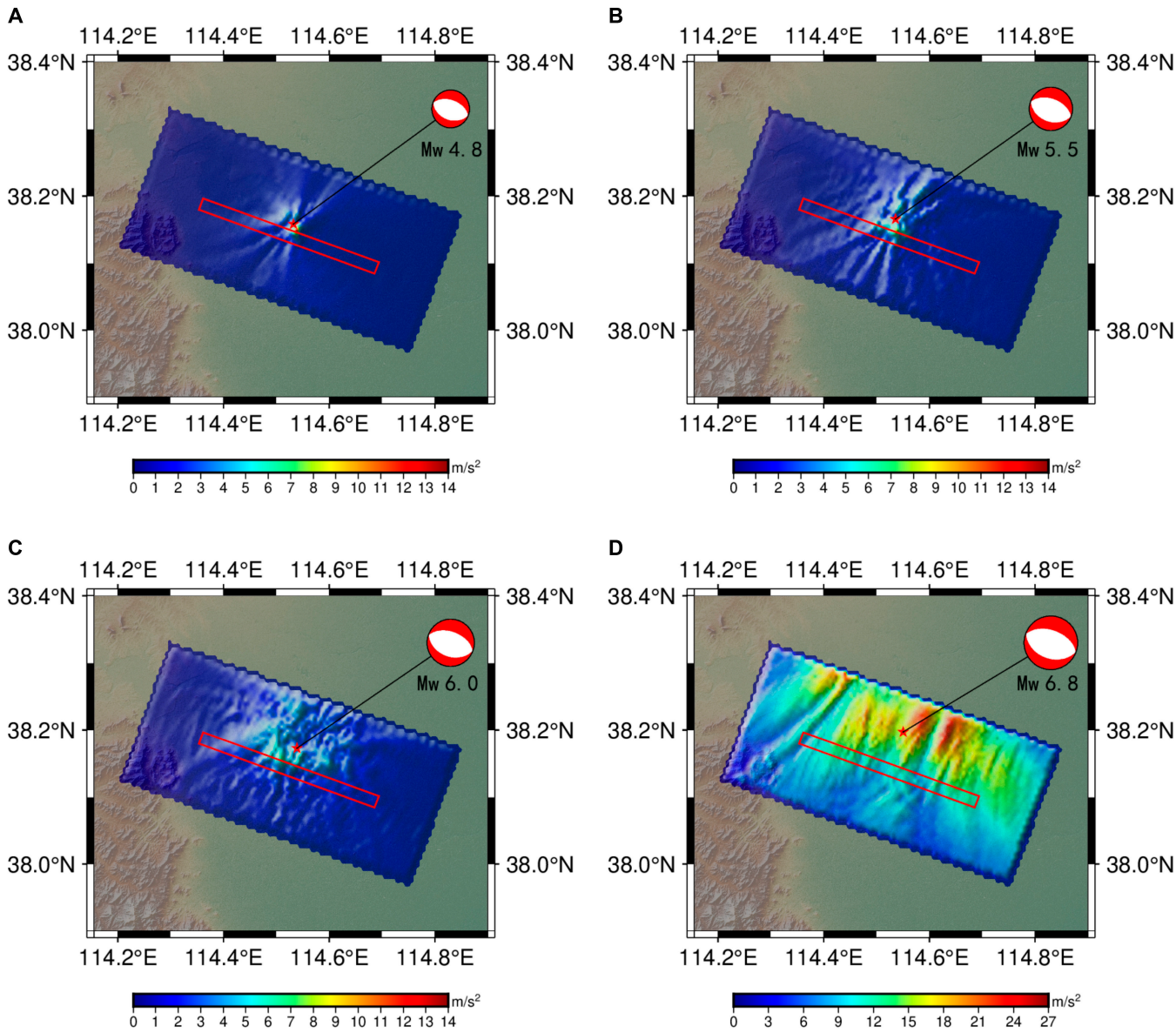

Fig. 5. ShakeMaps of the spatial ground motion fields (m/s^2): (A) service level earthquake, (B) design basis earthquake, (C) maximum considered earthquake, and (D) maximum credible earthquake. The inclined rectangle represents the simulation region; the red star indicates the epicenter location; the red rectangle delineates the near-fault area around the bridge site, from which ground motions are selected.

Table 3. Curvature ductility ratio quantitative information for the damage states at the base of the main tower

Damage states	Condition of reinforced concrete	Curvature ductility ratio range
Slight damage	Yielding of outermost reinforcement	$1 \le \mu_\phi < 1.3$
Moderate damage	Knee point of bilinear curve	$1.3 \le \mu_\phi < 2$
Extensive damage	Compressive strain of the edge concrete in the bridge tower reaches 0.004	$2 \le \mu_\phi < 6.1$
Complete damage	The concrete is crushed at the compressive edge of the section	$\mu_\phi \ge 6.1$

As shown in Fig. 6, the MIDA results are generally lower than those of IDA at equivalent PGA levels. In MIDA, the structure first enters the nonlinear stage at a PGA of 0.7*g*, at which point the response exceeds the moderate damage threshold. Therefore, the PGA values corresponding to the slight and moderate damage onset are considered to be 0.7*g*, and the PGA

associated with the extensive damage stage is identified as 0.9*g*; meanwhile, no complete damage is observed. For IDA, the structure first reaches the slight, moderate, extensive, and complete damage stages at PGA levels of 0.5*g*, 0.5*g*, 0.6*g*, and 0.8*g*, respectively. In terms of the inflection point of the results (i.e., the PGA amplitude at which the structure enters the nonlinear stage), those of MIDA and IDA appear at approximately 0.7*g* and 0.5*g*, respectively. This discrepancy is primarily due to 2 inherent IDA limitations: (a) subjectivity and arbitrariness in ground motion selection and (b) distortion introduced through amplitude scaling. For instance, pulse-like near-fault motions, which typically occur in moderate-to-large magnitude events [16,17], are often inappropriately scaled down to lower intensity levels, leading to unrealistically severe structural responses and premature nonlinearity onset. Given that researchers often strive to include a diverse set of ground motions in IDA analyses [1,51], such cases occur frequently.

This inherent tendency in IDA to combine a broad spectrum of ground motions, including records from different seismic events and distances, directly contributes to the larger dispersion observed in its results. As shown in Fig. 6, when the input PGA is below 0.5*g*, the response dispersion in MIDA and IDA is relatively low, with IDA exhibiting only slightly higher dispersion. Because the structure behaves essentially elastically in this range, the impact on seismic performance assessment is limited. However, once the input PGA exceeds 0.5*g* and the structure enters the nonlinear stage, the IDA response dispersion increases markedly and surpasses that of MIDA. This divergence is mainly due to the inconsistent nature of ground motion inputs in IDA. Structural damage may occur at different PGA levels for each ground motion record, not because of their intrinsic randomness but because of the inconsistencies introduced by subjective selection and scaling. Specifically, the wide range of motion types included in IDA analyses results in substantial structural demand dispersion, unrelated to the actual hazard scenario under consideration. Consequently, IDA yields a much more scattered picture of when and how the structure transitions into the nonlinear stage, consistent with previous studies [52–54]. At a PGA level of approximately 1.4*g*, most ground motions in IDA lead to complete damage whereas the structure remains with extensive damage under the same input intensity in MIDA. This contrast is largely attributed to the inherent differences in ground motion generation. In MIDA, all input motions are simulated for the same magnitude scenario, reflecting consistent source and site characteristics. Meanwhile, IDA combines records from disparate events and applies uniform amplitude scaling, which introduces nonphysical variability and results in a wider structural response dispersion.

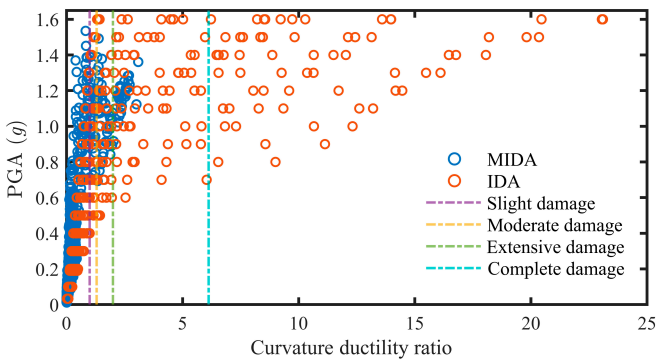

Fig. 6. Scatter plot of tower base curvature ductility ratio.

Figure 7 shows the 50th, 16th, and 84th percentile curves of the curvature ductility ratio at the tower base [32], along with the corresponding box plots under various seismic hazard levels. The mean, standard deviation, and COV for the curvature ductility ratio under service level, design basis, maximum considered, and maximum credible earthquakes are summarized in Table 4.

As shown in Fig. 7, under service level, design basis, and maximum considered earthquakes, the 84th percentile of the curvature ductility ratio at the tower base remains below 1 in both MIDA and IDA, indicating that the structure stays within the elastic stage. For maximum credible earthquakes, the 84th percentile value remains below 2 in MIDA, suggesting that the structure avoids extensive damage. Meanwhile, the corresponding IDA value exceeds 2, indicating extensive damage onset. These results demonstrate that IDA based on historical ground motion records tends to be much more conservative in seismic performance assessment.

As illustrated in Fig. 7 and Table 4, MIDA exhibits greater dispersion than IDA under low seismic hazard levels, such as the service level earthquake. This is primarily because low-magnitude earthquakes correspond to relatively small fault

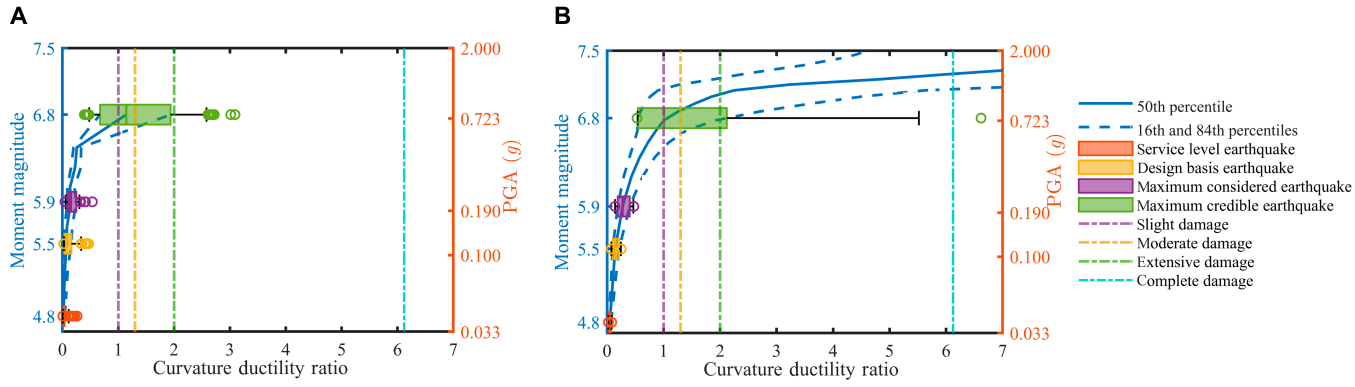

Fig. 7. Comparison of the MIDA and IDA results. (A) 50th, 16th, and 84th percentile curves of the tower base curvature ductility ratio obtained from MIDA, and the modified boxplots of the curvature ductility ratio under ground motions of different seismic intensity levels. (B) 50th, 16th, and 84th percentile curves of the tower base curvature ductility ratio obtained from IDA, and the modified boxplots of the curvature ductility ratio under ground motions of different seismic intensity levels. The lower and upper edges of each box represent the 16th and 84th percentiles, respectively, covering approximately 68% of the data. The central line indicates the median (50th percentile). Whiskers span from the 5th to the 95th percentiles, and outliers beyond this range are shown as hollow circles.

Table 4. Mean, standard deviation, and COV for curvature ductility ratios

Method	Statistic measure	Service level earthquake	Design basis earthquake	Maximum considered earthquake	Maximum credible earthquake
MIDA	Mean	0.035	0.109	0.161	1.313
	Standard deviation	0.043	0.098	0.081	0.676
	COV	1.222	0.906	0.500	0.515
IDA	Mean	0.048	0.147	0.279	1.559
	Standard deviation	0.018	0.055	0.103	1.486
	COV	0.370	0.371	0.371	0.953

rupture areas, which produce spatially limited high-intensity zones. Consequently, the ground motions sampled from the near-fault region vary more markedly in amplitude, leading to higher structural response dispersion. However, this variability reflects the natural spatial heterogeneity of ground motions and should not be considered artificial. Meanwhile, IDA appears more stable at low intensity levels, largely because its input records are uniformly scaled, masking the underlying variability of ground motion characteristics.

The dispersion in MIDA decreases markedly as the seismic intensity increases and eventually stabilizes at higher hazard levels. Meanwhile, the dispersion in IDA increases markedly, especially in the nonlinear range. In the maximum credible earthquake scenario, the COV in IDA reached 95.3%, nearly twice that of MIDA (51.5%). This rapid increase results from inconsistent ground motion selection and nonphysical scaling in IDA, which introduces artificial dispersion unrelated to the actual seismic hazard. MIDA offers a more realistic and robust basis for assessing seismic reliability under extreme ground motion scenarios by preserving the physical coherence of input motions across all intensity levels.

Discussion

This study proposes the MIDA method to assess the seismic performance of structures under realistic near-fault earthquake scenarios. MIDA enables the direct incorporation of magnitude-dependent seismic inputs that accurately reflect site-specific hazard conditions and fault rupture characteristics by integrating a source-to-site-to-structure simulation approach and using physics-based ground motion generation.

A comparative evaluation using the curvature ductility ratio at the tower base shows that MIDA consistently predicts lower demands than conventional IDA for the same PGA values. Moreover, the PGA threshold at which the structure enters the nonlinear stage is lower in IDA than in MIDA. Considering the subjectivity and uncertainty associated with ground motion selection in IDA, MIDA provides a more reliable and physically consistent assessment of structural capacity by leveraging magnitude-specific ground motions reflective of realistic source and site conditions.

IDA is affected by the subjectivity and uncertainty in ground motion selection as well as the distortions introduced through amplitude scaling. These issues result in substantially greater structural response variability, especially in the nonlinear stage. In the maximum credible earthquake scenario, the COV in IDA reaches 0.953, approximately 2.57 times the value in the maximum considered earthquake scenario. Meanwhile, the corresponding COV in MIDA is 0.515, representing a relatively steady uncertainty in the response. This highlights MIDA's ability to provide stable and physically meaningful estimates of structural performance, especially under extreme seismic scenarios.

For the cable-stayed bridge investigated in this study, MIDA results show that the tower does not reach the threshold of slight damage under service level, design basis, and maximum considered earthquake scenarios, indicating that the structure possesses strong seismic capacity and a high safety reserve level. However, in the maximum credible earthquake scenario, IDA predicts extensive or complete damage in many cases whereas MIDA indicates that the structure remains within acceptable performance limits. These results demonstrate that IDA tends to underestimate the true seismic structural capacity in practice.

In summary, the proposed MIDA method accurately represents near-field characteristics of ground motion at engineering sites, effectively overcoming 2 fundamental shortcomings of conventional IDA: the subjectivity in ground motion selection and distortion due to amplitude scaling. MIDA provides a more robust, realistic, and hazard-consistent evaluation of structural seismic performance by eliminating these sources of bias. Therefore, this study fills a critical methodological gap in current performance-based assessment practices and offers a practical path forward for improving the seismic reliability analysis of critical structures in near-fault environments.

Acknowledgments

Funding: This research was supported by the National Natural Science Foundation of China (Grant No. 52378171), the Scientific Research Project of Higher Education Institutions in Hebei Province (Grant No. CXZX2025050), the Natural Science Foundation of Hebei Province (CN) (Grant Nos. E2022210095 and E2024210049), and the S&T Program of Hebei (CN) (Grant No. 216Z5402G).

Author contributions: C.L. conceived and developed the methodology. J.L. performed the formal analysis, carried out the validation, and wrote the initial version of the manuscript. H.W. administered the project and contributed to funding acquisition. X.R. and X.W. provided resources. All authors contributed to the revision process and provided comments on different versions of the manuscript. All authors have approved the publication version.

Competing interests: The authors declare that they have no competing interests.

Data Availability

All data generated or analyzed during this study are available at https://doi.org/10.5281/zenodo.16629489. The code of SW4 (Seismic Waves, 4th order) was downloaded from https://github.com/geodynamics/sw4. The Generic Mapping Tools for generating some figures are available at https://github.com/GenericMappingTools. All data needed to evaluate the conclusions in the paper are present in the paper.

References

1. Vamvatsikos D, Cornell CA. Incremental dynamic analysis. *Earthq Eng Struct Dyn*. 2002;31(3):491–514.
2. Vamvatsikos D, Cornell CA. Applied incremental dynamic analysis. *Earthquake Spectra*. 2004;20(2):523–553.
3. Billah AM, Alam MS. Seismic performance evaluation of multi-column bridge bents retrofitted with different alternatives using incremental dynamic analysis. *Eng Struct*. 2014;62:105–117.
4. Di Trapani F, Malavisi M. Seismic fragility assessment of infilled frames subject to mainshock/aftershock sequences using a double incremental dynamic analysis approach. *Bull Earthq Eng*. 2019;17(1):211–235.
5. Wen T, Jiang L, Jiang L, Zhou W, Du Y. Optimal intensity measure selection in incremental dynamic analysis: Methodology improvements and application to a high-speed railway bridge. *Bull Earthq Eng*. 2024;22(4):2059–2083.
6. Medina RA, Krawinkler H. Evaluation of drift demands for the seismic performance assessment of frames. *J Struct Eng*. 2005;131(7):1003–1013.
7. Dolšek M. Incremental dynamic analysis with consideration of modeling uncertainties. *Earthq Eng Struct Dyn*. 2009;38(6):805–825.
8. Kiani J, Khanmohammadi M. New approach for selection of real input ground motion records for incremental dynamic analysis (IDA). *J Earthq Eng*. 2015;19(4):592–623.
9. Zhou Y, Ge P, Han J, Lu Z. Vector-valued intensity measures for incremental dynamic analysis. *Soil Dyn Earthq Eng*. 2017;100:380–388.
10. Yang J, Zhuang H, Zhang G, Tang B, Xu C. Seismic performance and fragility of two-story and three-span underground structures using a random forest model and a new damage description method. *Tunn Undergr Space Technol*. 2023;135:Article 104980.
11. Zacharenaki A, Fragiadakis M, Assimaki D, Papadrakakis M. Bias assessment in incremental dynamic analysis due to record scaling. *Soil Dyn Earthq Eng*. 2014;67:158–168.
12. Yazdani M, Jahangiri V, Marefat MS. Seismic performance assessment of plain concrete arch bridges under near-field earthquakes using incremental dynamic analysis. *Eng Fail Anal*. 2019;106:Article 104170.
13. Pang Y, Cai L, Zhong J. Seismic performance evaluation of fiber-reinforced concrete bridges under near-fault and far-field ground motions. *Structure*. 2020;28:1366–1383.
14. Sehhati R, Rodriguez-Marek A, ElGawady M, Cofer WF. Effects of near-fault ground motions and equivalent pulses on multi-story structures. *Eng Struct*. 2011;33(3):767–779.
15. Tzimas AS, Kamaris GS, Karavasilis TL, Galasso C. Collapse risk and residual drift performance of steel buildings using post-tensioned MRFs and viscous dampers in near-fault regions. *Bull Earthq Eng*. 2016;14(6):1643–1662.
16. Dabaghi M, Der Kiureghian A. Stochastic model for simulation of near-fault ground motions. *Earthq Eng Struct Dyn*. 2017;46(6):963–984.
17. Somerville PG, Smith NF, Graves RW, Abrahamson NA. Modification of empirical strong ground motion attenuation relations to include the amplitude and duration effects of rupture directivity. *Seismol Res Lett*. 1997;68(1):199–222.
18. Luco N, Bazzurro P. Does amplitude scaling of ground motion records result in biased nonlinear structural drift responses? *Earthq Eng Struct Dyn*. 2007;36(13):1813–1835.
19. Grigoriu M. To scale or not to scale seismic ground-acceleration records. *J Eng Mech*. 2011;137(4):284–293.
20. Latečki H, Molinari I, Stipčević J. 3D physics-based seismic shaking scenarios for city of Zagreb, capital of Croatia. *Bull Earthq Eng*. 2022;20(1):167–192.
21. Girmay N, Poulos A, Miranda E. Evaluation of directionality in physics-based ground motion simulations of strike-slip earthquakes. *Earthquake Spectra*. 2025;41(1):436–456.
22. Kenawy M, McCallen D, Pitarka A. Characteristics and selection of near-fault simulated earthquake ground motions for nonlinear analysis of buildings. *Earthquake Spectra*. 2023;39(4):2281–2322.
23. Wang F, Zhang Y, Lin X, Ba Z. City-scale buildings damage estimation based on broadband physics-based ground motion simulation of 2021 Ms 6.4 Yangbi, China, earthquake. *Earthquake Spectra*. 2023;40(1):446–468.
24. Gatti F, Touhami S, Lopez-Caballero F, Paolucci R, Clouteau D, Fernandes VA, Kham M, Voldoire F. Broadband 3-D earthquake simulation at nuclear site by an all-embracing source-to-structure approach. *Soil Dyn Earthq Eng*. 2018;115:263–280.
25. Wang XC, Wang JT, Zhang CH. Deterministic full-scenario analysis for maximum credible earthquake hazards. *Nat Commun*. 2023;14(1):6600.
26. Diao FQ, Weng HH, Ampuero J-P, Shao ZG, Wang RJ, Long F, Xiong X. Physics-based assessment of earthquake potential on the Anninghe-Zemuhe fault system in southwestern China. *Nat Commun*. 2024;15(1):6908.
27. McCallen D, Petersson A, Rodgers A, Pitarka A, Miah M, Petrone F, Sjögreen B, Abrahamson N, Tang H. EQSIM—A multidisciplinary framework for fault-to-structure earthquake simulations on exascale computers. Part I: Computational models and workflow. *Earthquake Spectra*. 2021;37(2):707–735.
28. McCallen D, Petrone F, Miah M, Pitarka A, Rodgers A, Abrahamson N. EQSIM—A multidisciplinary framework for fault-to-structure earthquake simulations on exascale computers. Part II: Regional simulations of building response. *Earthquake Spectra*. 2021;37(2):736–761.
29. Rosti A, Smerzini C, Paolucci R, Penna A, Rota M. Validation of physics-based ground shaking scenarios for empirical fragility studies: The case of the 2009 L'Aquila earthquake. *Bull Earthq Eng*. 2023;21(1):95–123.
30. Pang Y, Cai L, Ouyang H, Zhou X. Seismic performance assessment of different fibers reinforced concrete columns using incremental dynamic analysis. *Constr Build Mater*. 2019;203:241–257.

31. Perraud Y, Chatzigogos CT, Meza-Fajardo KC, Labbé P. Effect of Rayleigh waves on seismic response of bridge pylons via incremental dynamic analyses. *Soil Dyn Earthq Eng*. 2022;152:Article 107043.
32. Jalayer F, Cornell CA, A technical framework for probability-based demand and capacity factor (DCFD) seismic formats. Pacific Earthquake Engineering Center, University of California, Berkeley; 2003.
33. Kuhlemeyer RL, Lysmer J. Finite element method accuracy for wave propagation problems. *J Soil Mech Found Div*. 1973;99(5):421–427.
34. Sjögreen B, Petersson NA. A fourth-order accurate finite difference scheme for the elastic wave equation in second-order formulation. *J Sci Comput*. 2012;52(1):17–48.
35. Petersson NA, Sjögreen B. SW4, version 2.0. Davis (CA): Computational Infrastructure of Geodynamics; 2017.
36. Petersson NA, Sjögreen B. Users guide to SW4, version 2.0. Livermore (CA): Lawrence Livermore National Laboratory; 2017.
37. Graves RW, Pitarka A. Broadband time history simulation using a hybrid approach. In *Proceedings of 13th World Conference on Earthquake Engineering.* Vancouver (Canada): International Association for Earthquake Engineering; 2004.
38. Graves RW, Pitarka A. Broadband ground-motion simulation using a hybrid approach. *Bull Seismol Soc Am*. 2010;100(5A):2095–2123.
39. Graves R, Pitarka A. Refinements to the Graves and Pitarka (2010) broadband ground-motion simulation method. *Seismol Res Lett*. 2015;86(1):75–80.
40. Graves R, Pitarka A. Kinematic ground-motion simulations on rough faults including effects of 3D stochastic velocity perturbations. *Bull Seismol Soc Am*. 2016;106(5):2136–2153.
41. Pitarka A, Graves R, Irikura K, Miyakoshi K, Rodgers A. Kinematic rupture modeling of ground motion from the M7 Kumamoto, Japan earthquake. *Pure Appl Geophys*. 2020;177(5):2199–2221.
42. Pitarka A, Graves R, Irikura K, Miyakoshi K, Wu C, Kawase H, Rodgers A, McCallen D. Refinements to the Graves–Pitarka kinematic rupture generator, including a dynamically consistent slip-rate function, applied to the 2019 mw 7.1 Ridgecrest earthquake. *Bull Seismol Soc Am*. 2022;112:287–306.
43. General Administration of Quality Supervision, Inspection and Quarantine of the People's Republic of China, Standardization Administration of the People's Republic of China, *Seismic ground motion parameters zonation map of China: GB 18306-2015.* Beijing: Standards Press of China; 2015.
44. Zhang LX, editor. GB/T 17742-2020 Training and Implementation Guide for the "China Seismic Intensity Scale". Beijing: Seismological Press; 2021. p. 131.
45. Li SB, *Chinese earthquakes*. Beijing: Seismological Press; 2018. p. 207.
46. Sha HJ, Lu YJ. Statistical relationship between surface wave magnitude and moment magnitude of China seismograph network. *Chin J Seismol Geomagn Obs Res*. 2018;39(1):31–36.
47. Wells DL, Coppersmith KJ. New empirical relationships among magnitude, rupture length, rupture width, rupture area, and surface displacement. *Bull Seismol Soc Am*. 1994;84(4):974–1002.
48. Ministry of Transport of the People's Republic of China, *Code for seismic design of highway bridges: JTG/T 2231-01-2020.* Beijing: China Communications Press; 2020.
49. Pacific Earthquake Engineering Research Center (PEER), Strong motion database. [accessed 2025] https://ngawest2.berkeley.edu
50. Hose Y, Silva P, Seible F. Development of a performance evaluation database for concrete bridge components and systems under simulated seismic loads. *Earthquake Spectra*. 2012;16(2):413.
51. Federal Emergency Management Agency (FEMA), FEMA P695: Quantification of Building Seismic Performance Factors. Washington (DC): Federal Emergency Management Agency; 2009.
52. Vamvatsikos D, Cornell CA. Direct estimation of seismic demand and capacity of multidegree-of-freedom systems through incremental dynamic analysis of single degree of freedom approximation. *J Struct Eng*. 2005;131(4):589–599.
53. Asgarian B, Sadrinezhad A, Alanjari P. Seismic performance evaluation of steel moment resisting frames through incremental dynamic analysis. *J Constr Steel Res*. 2010;66(2):178–190.
54. Dizaj EA, Salami MR, Kashani MM. Seismic vulnerability analysis of irregular multi-span concrete bridges with different corrosion damage scenarios. *Soil Dyn Earthq Eng*. 2023;165:Article 107678.

Civil Engineering Sciences

A Magnitude-Based Incremental Dynamic Analysis Method for Seismic Performance Assessment of Near-Fault Structures

Chao Luo, Jingjing Li, Hao Wang, Xueliang Rong, and Xiaoshan Wang

Citation: Luo C, Li J, Wang H, Rong X, Wang X. A Magnitude-Based Incremental Dynamic Analysis Method for Seismic Performance Assessment of Near-Fault Structures. *Civ Eng Sci*. 2026;**2**:0011. DOI: 10.34133/cesci.0011

Seismic performance assessment of near-fault critical structures remains challenging, as conventional intensity-based incremental dynamic analysis (IDA) approaches suffer from subjective ground motion selection and nonphysical amplitude scaling, which introduce artificial dispersion and compromise performance assessment reliability. This study proposes a magnitude-based incremental dynamic analysis (MIDA) method that replaces empirical record selection and scaling with physically consistent ground motion simulations conditioned on earthquake magnitude. Various earthquake scenarios, ranging from service level to maximum considered earthquakes, are simulated, and the curvature ductility ratio at the tower base is adopted as the damage measure to evaluate the seismic performance of a near-fault cable-stayed bridge. Results indicate that MIDA yields markedly lower dispersion and improved physical consistency in structural responses than IDA after entering the nonlinear stage. In maximum credible earthquake scenarios, the coefficient of variation of structural response reaches 95.3% in IDA but is only 51.5% in MIDA, highlighting the improved reliability and accuracy of seismic performance assessment. By addressing the critical limitations of conventional IDA approaches, MIDA substantially enhances the physical consistency and precision of seismic performance assessments for near-fault structures. It offers a scalable methodological basis for consistent seismic performance evaluation and supports reliability-informed engineering decision-making in near-fault hazard zones.
Image

Civil Engineering Sciences (ISSN 3067-7807) is published by the American Association for the Advancement of Science. 1200 New York Avenue NW, Washington, DC 20005.